applied sciences

MDPI

Article

Study on the Creep of Damage-Containing Anthracite: Theory and Experiment

Gang Li [1], Guochao Yan [1,*], Shaoqi Kong [1,*], Xuyang Bai [1], Chaofei Du [2], Jiajun Li [1] and Jiawei Zhang [1]

[1] College of Mining Engineering, Taiyuan University of Technology, Taiyuan 030024, China
[2] College of Mechanical Engineering, Chongqing University of Technology, Chongqing 400054, China
* Correspondence: ygc15534471030@163.com (G.Y.); kongshaoqi@tyut.edu.cn (S.K.)

Abstract: Fractal derivatives characterize the accelerated creep phase of the creep process. In this study, based on the fractal order theory, the integer-order derivatives are defined from the spatio-temporal self-similarity phenomenon of the dynamic process using the scale change method, and the viscoplastic model is improved to establish a new creep instantonal model with damage to describe the complete creep phase of anthracite. The effects of damage variables on initial and accelerated creep were investigated by performing graded-loading creep tests. Based on the experimental data, inversions of the model-related parameters were performed, and parameter sensitivities were analyzed. The results show that the proposed model can better characterize the complete creep process of anthracite coal, which verifies the correctness and rationality of the model. The damage content affects the initial and accelerated creep strain under different loading levels, and a specific functional relationship exists between them. The study's findings can provide some reference material for the stability control of anthracite affected by disturbing stresses.

Keywords: anthracite; fractal derivatives; improved viscoplastic model; damage-containing creep intrinsic structure model; model validation

Citation: Li, G.; Yan, G.; Kong, S.; Bai, X.; Du, C.; Li, J.; Zhang, J. Study on the Creep of Damage-Containing Anthracite: Theory and Experiment. *Appl. Sci.* **2023**, *13*, 8691. https://doi.org/10.3390/app13158691

Academic Editors: José António Correia and Nikolaos Koukouzas

Received: 7 May 2023
Revised: 7 July 2023
Accepted: 26 July 2023
Published: 27 July 2023

1. Introduction

Creep behavior has existed in deep subsurface rocks for a long time and is not easy to detect [1,2]. The study of rock creep behavior is of great importance for the mechanical properties of rocks. Many scholars have focused on this topic and achieved great results [3–10]. Rock models of limestone, sandy mudstone, and saltstone have been continuously revealed and improved, and rock models under different conditions have been explored. In the deep mining of rocks, various complex tunnels frequently occur [11–14]. Due to the superposition of mining stresses and the natural influence of the presence of deep rocks, the rocks are more likely to exhibit the characteristics of creep behavior [15–18]. Anthracite, a high-ranking coal, has the highest carbon content and the fewest impurities [19]. Its random combination of carbon atoms makes anthracite more prone to deformation under horizontal stresses. Therefore, it is valuable to propose a model to describe the creep process of anthracite.

Due to the complexity of the geological environment, it is difficult to predict the creep process of rocks. In recent years, scholars have conducted much research on coal rock bodies under different conditions and provided a theoretical basis for the long-term stability of underground projects through experimental comparisons, numerical simulation, and theoretical calculations, while Falaleev [20] evaluated rock creepiness. Khoshghalb [21] reviewed the traditional experimental creep test, discussed possible sources of inaccuracy in the test results, and made relevant recommendations. Wu et al. [22] studied the effect of structural anisotropy on the rheological behavior of ultra-deep hard rocks, considering the rock's metrological deformation. The results show that hard rocks do not exhibit an accelerated creep phase, and the deformation rate and shrinkage ratio show that creep behavior is

more influenced by structural anisotropy. Mansouri et al. [23] investigate the effect of the microstructural evolution of salt rocks on strain behavior. Constant displacement rate tests on creep specimens show that the strain profile has a moderate strain-hardening characteristic. Peng et al. [24] conducted triaxial creep experiments on mudstone, introduced the meshless method, and derived a new meshless algorithm formulation. Huang et al. [25] conducted an experimental study of siltstone based on a new experimental apparatus that simulates dynamic impact loading using the free fall of weights, which provides high static stresses over a long period. The results show that rock creep disturbance deformation exhibits a continuous developmental phase. Liu et al. [26] developed a numerical simulation of multi-stage loading in Flac3D software, and the calculated results were in better agreement with the test data. Zhu et al. [27] proposed the intrinsic law of rock damage under multiple strain rates and performed numerical simulations of dynamic loading and rheological disturbances to elucidate the rock damage behavior for different combinations of strain rates. Zhang et al. [28] developed a numerical procedure based on the discontinuous deformation analysis method, considering the shear in the structural plane. The numerical procedure was established using the discontinuous deformation analysis method, considering shear deformation within the structure's surface. The effectiveness of the DDA extension method is demonstrated. Tang et al. [29] proposed a new quadratic creep model based on the damage mechanics of continuous media and variable-order fractional derivatives. Liu et al. [30] analyzed the creep law of deeply saturated rocks and proposed the Schofield–Scott–Blair model based on joint rheology. Wan et al. [31] investigated the creep properties of amphiboles using the cyclic incremental-step-loading method. They combined the generalized Kelvin creep model with the Mohr–Coulomb criterion to derive the corresponding viscous–elastic–plastic transient relationship. In general, the creep behavior of rocks has been subjected to many experiments. However, creep tests on coal are uncommon, especially for higher-order coals, such as anthracite.

The creep properties of coal are very different from those of rocks, such as sandstone, limestone, etc. Compared to substances with higher load-bearing strength, coal is more susceptible to deformation by slight stress perturbations due to its physical properties. From a microscopic point of view, anthracite, a higher-order coal, has a more complex arrangement of carbon atoms due to its higher carbon content. In general, the creep properties of anthracite coal are more complex. In summary, a new viscoplastic model is proposed in this paper based on fractal order derivatives. By introducing damage variables combined with the viscoplastic model, a new fractal-order intrinsic model for anthracite containing damage is proposed, which can describe the complete creep process of anthracite. Then, a series of experiments are conducted on anthracite coal, and the inverse fitting of the relevant parameters of the model under different stress-level conditions is carried out based on the experimental data to verify the applicability and reasonability of the model. Finally, the sensitivity of the parameters is analyzed in detail.

2. Fractal Order Model Construction

2.1. Fractal Order Newton Body with Damage

Based on the study of typical geotechnical intrinsic models, fractional order theory is widely used [32–34]. In terms of a mathematical definition, the fractional order derivative, an integral over the time kernel function, can better describe the evolution of the dynamic process under the global effect. In contrast, the fractional derivative is based on local effects, and its functional model is relatively simple. Starting from the phenomenon of spatio-temporal self-similarity of the dynamical process, the fractal derivative is defined using the scale-variation method for integer-order derivatives. If the original function is invariant in form at any scale, then

$$\frac{df(t)}{dt^q} = \lim_{t \to t'} \frac{f(t) - f(t')}{t^q - t'^q}, \tag{1}$$

where q denotes the time-dependent order.

Based on the conventional creep model, the model generally exhibits significant damage characteristics during the accelerated creep phase. This is caused by damage at different stages of creep. From a microscopic point of view, this is due to the internal unit damage of the model. With the accumulation of damage to the unit cell inside the model, the model surface exhibits macroscopic cracking characteristics. The damage variable D is introduced to represent the damage of the unit cell, as follows:

$$D = 1 - \frac{N(t)}{N_0}, \tag{2}$$

where $N(t)$ denotes the number of intact cells in the time range t, and N_0 denotes the total number of cells.

As defined by Krajcinovic [35],

$$\frac{dN(t)}{dt} = -A(\sigma)N(t), \tag{3}$$

where A denotes the damage factor related to σ.

If the initial moment $N(0)$ is equal to N_0, then $D = 1 - e^{-At}$.

Based on the scale change method and the fractal derivative, $D = 1 - e^{-At^q}$.

According to the viscous pot expression of the fractional order theory, the Newton body stress σ(t)–strain ε(t) relationship containing the fractal derivative of the damage can be expressed as follows:

$$\begin{cases} \sigma(t) = \eta_2 e^{-At^q} \frac{d\varepsilon(t)}{dt^q} \\ \varepsilon(t) = \frac{\sigma(t)}{A\eta_2}(e^{At^q} - 1) \end{cases}, \tag{4}$$

where η_2 denotes the viscosity coefficient of the fractal derivative Newton body.

2.2. Fractal Order Creep Model Considering the Effect of Damage

The creep properties of coal are very different from those of rocks, such as sandstone, limestone, etc. [36–39]. Compared to substances with higher load-bearing strength, coal is more susceptible to deformation by slight stress perturbations due to its physical properties. From a microscopic point of view, anthracite, a higher-order coal, has a more complex arrangement of carbon atoms due to its higher carbon content. In general, the creep properties of anthracite coal are more complex. Existing creep models cannot better describe the accelerated creep phase of damaged anthracite because the model's characterization of the accelerated creep phase is primarily a linear model with constant parameters. Based on the traditional creep model, the instantaneous elastic–elastic–viscoplastic model can better characterize the creep characteristics, and by improving the viscoplastic body on this basis, it is possible to establish a creep model conforming to the creep equation of the damage-containing anthracite coal. Figure 1 shows the diagram of the fractal order creep model considering the influence of damage, where σ(t) denotes the stress, E_1 and E_2 denote the elastic modulus of model parts I and II, respectively, η_1 and η_2 denote the viscous coefficients of model parts II and III, and σ_{s1} denotes the dilation stress of the model up to the accelerated creep stage.

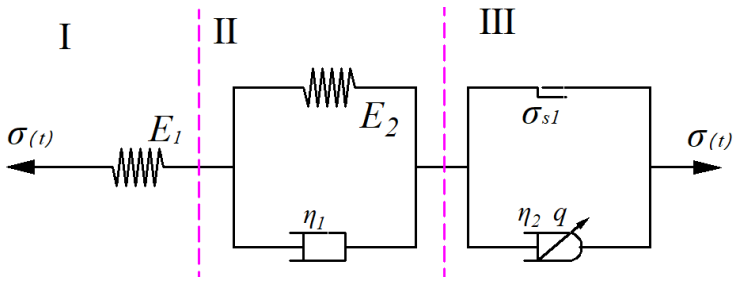

Figure 1. Diagram of fractal derivative creep model considering the effect of damage.

According to the basic principle of the model series–parallel connection,

$$\begin{cases} \sigma = \sigma_I = \sigma_{II} = \sigma_{III} \\ \varepsilon = \varepsilon_I + \varepsilon_{II} + \varepsilon_{III} \end{cases}, \tag{5}$$

When $\sigma < \sigma_{s1}$, the model I and II parts come into play to characterize the instantaneous creep deformation, deceleration creep deformation, and isokinetic creep deformation of anthracite creep deformation. The model equation of the state can be expressed as follows:

$$\begin{cases} \sigma_1 = E_1\varepsilon_1 \\ \sigma_2 = E_2\varepsilon_2 + \eta_1\dot{\varepsilon_2} \end{cases}, \tag{6}$$

According to the principle of the series–parallel connection of components and Equation (5), the model intrinsic equation in the one-dimensional state can be expressed as follows:

$$\sigma(t) = \frac{1}{E_1 + E_2}\left(E_1E_2\varepsilon_1 + E_1\eta_1\dot{\varepsilon_2} - \eta_1\dot{\sigma_2}\right), \sigma < \sigma_{s1}, \tag{7}$$

When $\sigma_{s1} \leq \sigma$, models I, II, and III characterize the instantaneous creep deformation, deceleration creep deformation, isokinetic creep deformation, and accelerated creep deformation of anthracite creep deformation. Based on the Newton body containing the fractal derivative of damage, the partial equation of the state of model III at this time can be expressed as follows:

$$\sigma - \sigma_{s1} = \eta_2 e^{-At^q}\frac{d\varepsilon(t)}{dt^q}, \sigma_{s1} \leq \sigma, \tag{8}$$

In summary, under different stress conditions, each part of the model is subjected to equal stress, and the total model strain is equal to the sum of each model strain. The joint solution of Equations (6)–(8) with the adaptive part of Equation (5), respectively, yields the model creep equation as follows:

$$\begin{aligned} \varepsilon(t)_1 &= \frac{\sigma}{E_1} + \frac{\sigma}{E_2}\left(1 - e^{-\frac{E_2}{\eta_1}t}\right), \sigma < \sigma_{s1} \\ \varepsilon(t)_2 &= \frac{\sigma}{E_1} + \frac{\sigma}{E_2}\left(1 - e^{-\frac{E_2}{\eta_1}t}\right) + \frac{\sigma - \sigma_{s1}}{\eta_2 A}\left(e^{At^q} - 1\right), \sigma \geq \sigma_{s1} \end{aligned} \tag{9}$$

2.3. Model 3D Extension

The 1D model considers only axial strain. In practical applications, anthracite coal is in a multi-directional stress state [40]. The deformation of anthracite coal can be better reflected by constructing a three-dimensional creep model. Based on the three-dimensional stress analysis of elastodynamics, the stress state of any unit inside the rock, i.e., the Corsi stress tensor σ_{ij}, can be expressed by the stress bias tensor S_{ij} and the stress sphere tensor σ_m. Among them, the plastic deformation of any unit body is affected by the stress deflection tensor, and the volume deformation of any unit body is represented by the stress sphere tensor σ_m.

$$\sigma_{ij} = \delta_{ij}\sigma_m + S_{ij}, \tag{10}$$

The strain tensor can be expressed as follows:

$$\varepsilon_{ij} = \delta_{ij}\varepsilon_m + e_{ij}, \tag{11}$$

where σ_m and ε_m denote the stress and strain spherical tensor, S_{ij} and e_{ij} denote the stress and strain bias tensor, and δ_{ij} is the Kronecker symbol for the unit tensor.

Based on the elasticity mechanics and one-dimensional Hooke's law, considering the material as a continuous medium and isotropic, the stress spherical tensor and bias tensor

are related to the strain spherical tensor and bias tensor, respectively, and the 3D Hooke body expression as follows:

$$\begin{cases} \sigma_m = 3K\varepsilon_m \\ S_{ij} = 2Ge_{ij} \end{cases}, \tag{12}$$

where K and G are the bulk modulus and elastic modulus, respectively, and $K = \frac{E}{3(1-2\mu)}$, $G = \frac{E}{2(1+\mu)}$, μ denotes Poisson's ratio.

During the triaxial test of anthracite coal, the sample is in the condition of equal surrounding pressure, i.e., the intermediate stress σ_{22} is equal to the minimum principal stress σ_{33}; then, the stress spherical tensor and the partial tensor can be expressed as follows:

$$\begin{cases} \sigma_m = \frac{1}{3}(\sigma_{11} + 2\sigma_{33}) \\ S_{ij} = \frac{2}{3}(\sigma_{11} - \sigma_{33}) \end{cases}, \tag{13}$$

Equations (12)–(14) are substituted into Equation (9) to obtain the creep equation under the 3D condition, which can be expressed as follows:

$$\begin{aligned} \varepsilon(t)_1 &= \tfrac{\sigma_{11}+2\sigma_{33}}{9K} + \tfrac{\sigma_{11}-\sigma_{33}}{3G_1} + \tfrac{\sigma_{11}-\sigma_{33}}{3G_2}\left(1 - e^{-\frac{G_2}{\eta_1}t}\right), \sigma_{11} - \sigma_{33} < \sigma_{s1} \\ \varepsilon(t)_2 &= \tfrac{\sigma_{11}+2\sigma_{33}}{9K} + \tfrac{\sigma_{11}-\sigma_{33}}{3G_1} + \tfrac{\sigma_{11}-\sigma_{33}}{3G_2}\left(1 - e^{-\frac{G_2}{\eta_1}t}\right) \\ &\quad + \tfrac{2\sigma_{11}-2\sigma_{33}-3\sigma_{s1}}{3\eta_2 A}\left(e^{At^q} - 1\right), \sigma_{11} - \sigma_{33} \geq \sigma_{s1} \end{aligned} \tag{14}$$

3. Creep Experiments

3.1. Equipment and Materials

All the test samples were taken from 0–120 m of the 3112 backwind chute of the Yangcheng Fuyan Coal Industry, Xiaoxi Coal Industry, Shanxi Province, China. According to the "Requirements for Engineering Rock Test Samples", the coal samples were sealed with cling film after being taken downhole to avoid weathering and dampness. The coal samples were processed using a ZS-100 drilling and coring machine, an SHM-200 double-sided smoothing machine, and a DQ-3 automatic rock slicer. To ensure that the parallelism of the end face was less than 0.02 mm and the flatness of the end face was less than 0.5 mm, the standard size of the coal sample was ϕ 50 mm $\times$ 100 mm. To study the effect of damage on anthracite coal creep, the RSM-SY5 intelligent acoustic wave meter was used for acoustic wave detection of the coal sample, and the sample with a small difference in wave velocity was selected for subsequent experiments. The wave velocity values were selected as 2000–2300 m/s to exclude the influence of existing sample cracks on the experimental results. After sample selection, samples were wrapped with cling film for maintenance.

3.2. Experimental Program

The creep process of anthracite coal was analyzed by considering the damage variables and the surrounding pressure factors. Among them, the elastic phase has less influence on the damage of coal samples, and it is necessary to ensure that the coal samples are loaded within the yield section to produce specific damage. The axial intermittent half-sine loading wave was used as the loading stress to prepare anthracite samples with different damage levels. The loading period was 1 s, and different ratios of loading stress time to unloading stress time indicated different damage variables. The control loading time did not exceed one-half of the loading period. Thus, with 0.1 s loading and 0.9 s unloading, the damage variable was 0.11; with 0.2 s loading and 0.8 s unloading, the damage variable was 0.25; with 0.3 s loading and 0.7 s unloading, the damage variable was 0.43; and with 0.4 s loading and 0.6 s unloading, the damage variable was 0.67. The ratio of loading and unloading was controlled between 0 and 1, consistent with the rules for defining the damage variable.

In this test, the MTS815.02 electro-hydraulic servo rock mechanics test system was used to perform graded-loading creep tests on the samples. The system had basic uniaxial,

conventional triaxial, and true triaxial test functions to meet the test requirements. The enclosing pressure was 90% of the peak anthracite stress strength as the total stress, and the graded equivalence was performed to determine the graded load. The first load level was 0.3 of the total stress, and the stresses at each level were 3.5 MPa, 4.4 MPa, 5.3 MPa, 6.2 MPa, 7.1 MPa, and 8.0 MPa. The creep preload time for each level was t = 50 h. The first level of stress in the specimen was loaded to 3.5 MPa under 0.05 MPa/s, and it was specified that when the axial displacement of the coal sample was <0.001 mm in 5 h, it reached equilibrium and applied the next level of load until the specimen was deformed and damaged. We plotted the whole creep axial process under different damage variables, as shown in Figure 2.

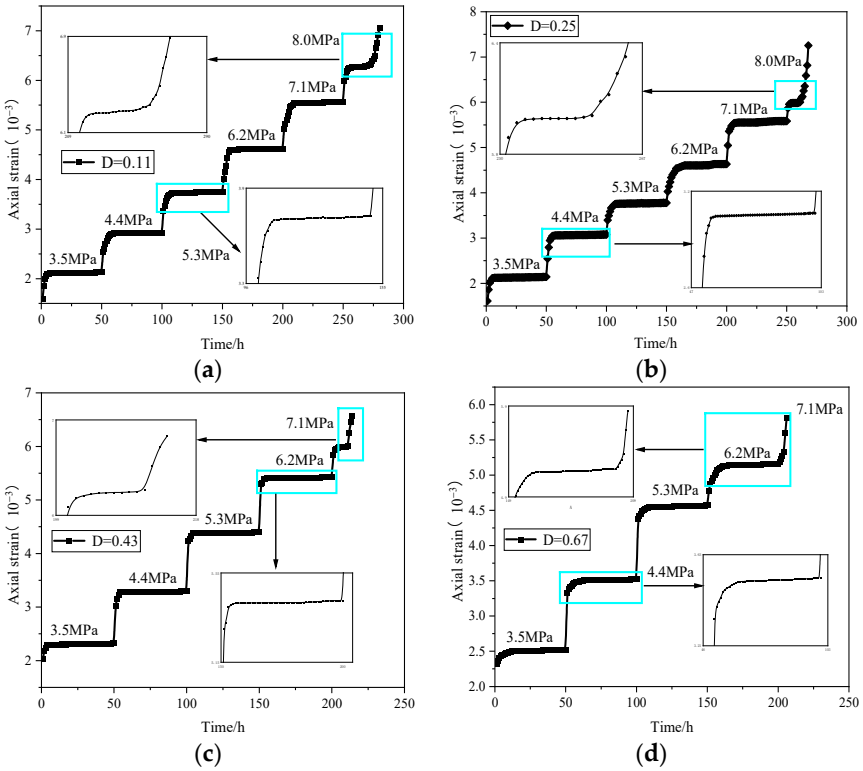

Figure 2. Creep axial process curve under different damage variables: (**a**) The damage variable is 0.11 to obtain the creep curve; (**b**) the damage variable is 0.25 to obtain the creep curve; (**c**) the damage variable is 0.43 to obtain the creep curve; (**d**) the damage variable is 0.67 to obtain the creep curve.

3.3. Analysis of Experimental Results

As shown in Figure 2, the anthracite exhibited complete creep behavior under the influence of low-damage variables. It can be seen that the anthracite creep is more stable in the first five stages as time progresses. The axial strain rises rapidly at the beginning of creep and gradually stabilizes after 1–3 h, with a slow increase in strain. During this time, the transient elasticity and elastoplasticity are more apparent, and the nonlinear behavior is more obscure, but this is very important to produce accelerated creep behavior. In the last creep stage, the strain rate increases significantly and exhibits an evident nonlinear characteristic. This phenomenon indicates that as the creep behavior proceeds, the damage to the internal unit body of anthracite coal accumulates and continuously absorbs external energy. The energy absorption reaches a critical value, and the damage destruction reaches a critical value and exhibits macroscopic damage characteristics.

4. Discussion

4.1. Parameter Fit

This section uses the damage variable D = 0.11 as an example to verify the fractal order anthracite creep Equation (14) based on the experimental creep data of six stages in Figure 2a. As shown in Figure 3, by fitting the creep Equation (14) and the fitted data curves, we can see that the first three stress levels can be compared together, and it is more evident that the fitted curves are in good agreement with the experimental data. The fitted correlation reaches 0.99 and above. The nonlinear behavior of the transient deformation phase, deceleration creep phase, and isokinetic creep phase of creep deformation can be well characterized. The initial creep phases of levels 4, 5, and 6 are nearly the same. It is worth noting that the fitted correlation of the last level reaches above 0.94, and the fitted curve model is more consistent with the experimental data. Comparing the fitted curves and experimental data, the proposed fractal order creep model can better characterize the total creep process of anthracite coal and better predict the nonlinear creep behavior of anthracite coal with time. The presently proposed model has some application value in predicting the creep strain of anthracite coal under different stress levels. Meanwhile, the relevant parameters fitted by the model are shown in Table 1, where R^2 denotes the fitted correlation coefficient.

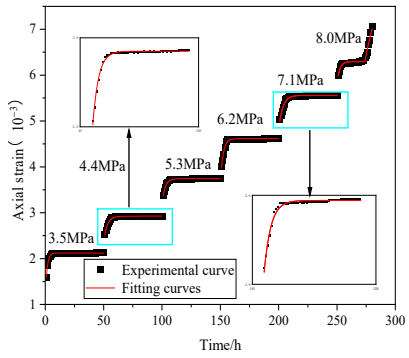

Figure 3. Model parameters and experimental data fit curve.

Table 1. Parameters of interest for model fitting.

	E_1(GPa)	E_2(GPa)	η_1(GPa·h)	η_2(GPa·h)	A	q	R^2
3.5 MPa	3.2531	3.3471	4.8421				0.995
4.4 MPa	1.8747	7.6149	22.5176				0.990
5.3 MPa	1.6709	9.2784	23.2373				0.993
6.2 MPa	1.7119	9.3656	27.9306				0.974
7.1 MPa	1.4773	9.4258	32.4143				0.977
8.0 MPa	1.3740	16.9105	39.6563	1.6933	0.0354	0.5209	0.945

4.2. Parameter Sensitivity Analysis

In order to better validate the rationality of the proposed model, this section provides a detailed analysis of the sensitivity of the relevant parameters in the model. It should be noted that the relevant parameters in the model are based on the Levenberg–Marquardt (L–M) optimization algorithm for regression inversion, which may not be considered the best method, but is conventional and reasonable. As shown in Table 1, six model parameters can be analyzed in detail.

4.2.1. Modulus of Elasticity E_1 and E_2

The elastic moduli E_1 and E_2 are the key parameters for the model to undergo transient and deceleration creep, and they contain specific physical significance. Analyzed from the functional point of view, this parameter controls the initial creep trend. From the perspective of damage, this parameter has a particular relationship with each stage of

damage and describes the evolution of anthracite damage. Figure 4a shows that the elastic modulus E_1 decreases with increasing stress, specifically from 3.2531 to 1.3740. The elastic modulus E_2 increases with increasing stress, from 3.3471 to 16.9105, as shown in Figure 4b. This can be explained by the increasing transient deformation with increasing stress levels. The model responds quickly to sudden loading and transitions to the decay creep phase and isokinetic creep phase.

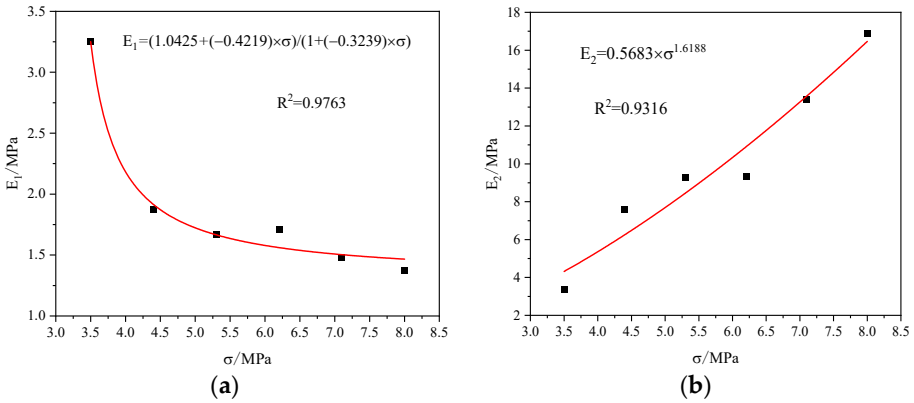

Figure 4. Elasticity model relationship curve.

4.2.2. Coefficient of Viscosity η_1

The viscosity coefficient mainly affects the isokinetic creep phase of the model. From the perspective of the function, this parameter controls the trend of the isokinetic creep phase; from the damage point of view, it increases from 4.8421 to 39.6543, reflecting the accumulation of damage energy. Importantly, it is essential for the model to produce an accelerated creep phase. Figure 5 shows the viscosity coefficient function relationship curve.

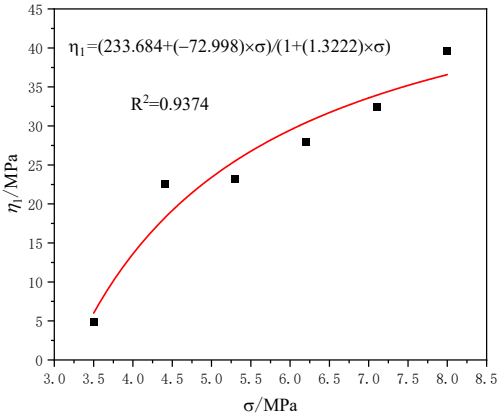

Figure 5. Viscosity coefficient function relationship curve.

4.2.3. Sensitivity of η_2, A, and q

In this section, we take the fitted data from Table 1 as reference values and fix two parameters separately to analyze the degree of variation of individual parameters on the strain. In Figure 6a, fixing the viscosity coefficient η_2 and the order q of 1.6933 and 0.5209, we analyze the sensitivity of the damage factor A. In Figure 6b, fixing the damage factor A and order q at 0.05 and 0.5209, we analyze the sensitivity of the viscosity factor η_2. In Figure 6c, the sensitivity of order q is explored by fixing the damage factor A and the sticking factor η_2 at 0.035 and 1.6933, respectively. We see that the viscosity coefficient η_2 and the damage factor A mainly affects the time of the model in the isokinetic creep phase, with a corresponding upward shift of the curve as the correlation coefficient decreases. This indicates that the parameters affect the time for the model to enter the accelerated creep phase, and the smaller the parameter, the faster the model enters the accelerated creep

phase. As shown in Figure 6, the curve shows a clear accelerated creep phase, indicating that the order q is the main factor that determines the rate of the accelerated creep phase. The order q has a lesser effect on the transient and decelerating creep phases. All three parameters have a specific functional relationship with the time and rate of the accelerated creep phase. This can be explained by the ability of this phase to respond quickly to sudden changes in model strain. In general, the fitted parameters obtained from the model are reasonable, and the validity and applicability of the model are also verified.

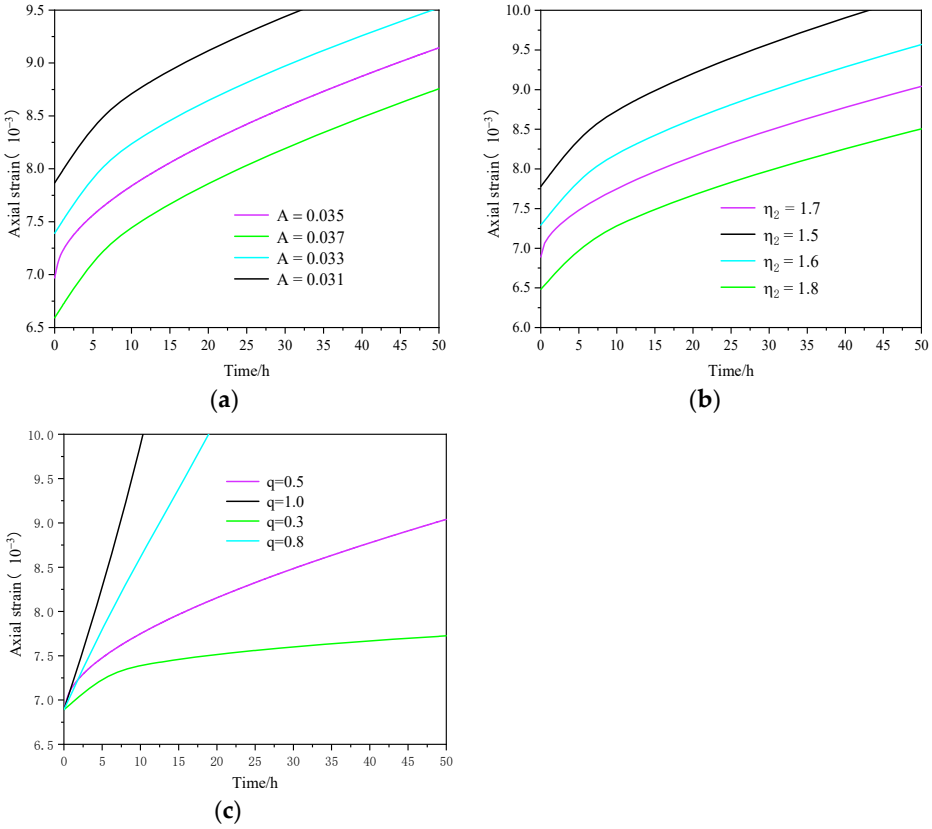

Figure 6. Curves of η_2, A, and q as a function of strain: (**a**) Sensitivity curve for damage factor A; (**b**) sensitivity curve for the viscosity factor η_2; (**c**) sensitivity curve for order q.

4.3. Effect of Different Damage Variables on Initial and Accelerated Creep

To better verify the effects of different damage variables on anthracite creep, we analyze them in this section. Damage variables are important indicators of the initial and accelerated creep of anthracite coal. Different damage variables have different effects on the initial and accelerated creep of anthracite coal. Based on the built-in equations of Origin software, the relationships between the effects of different damage variables on initial and accelerated creep were fitted. Figure 7 shows the relationship between initial and accelerated creep strains of anthracite coal and damage variables. As the damage variable increases, the initial creep strain of anthracite coal keeps increasing, and the growth rate decreases. This can be explained by the fact that the damage alters the microstructure of the internal unitary of the anthracite coal. The larger the initial damage, the more pronounced the microstructural damage. Under the loading of the initial stress, the microstructure changes show corresponding changes in macroscopic characteristics. It can be said that the damage to the internal unitary caused the creep strain of the anthracite coal. Meanwhile, the accelerated creep-phase strain of anthracite decreases to different degrees with the increase in damage variables. This can be explained by the fact that under loading at high stress levels, the energy absorbed by the unitary body is more easily released as the damage to the internal unitary body of anthracite accumulates. The unitary bodies are

more likely to cause macroscopic changes earlier, which is important for the characteristics of macroscopic changes caused by the final accelerated creep stage of anthracite.

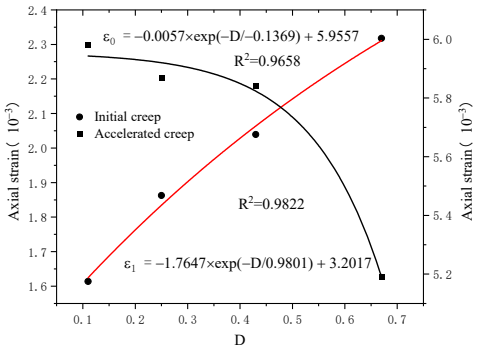

Figure 7. Curves of initial and accelerated creep strain as a function of damage variables.

For anthracite's creep mechanical properties, due to the restrictive experimental conditions, only the damage effects on the initial and accelerated creep stages are analyzed in this paper. There are still some limitations for complex geological conditions, such as high moisture and high temperature, being influenced by external human-made effects. To make the model applicable to various complex conditions, it is necessary to conduct future studies on anthracite coal under different conditions to make the model simple and effective.

5. Conclusions

By analyzing the anthracite creep model and the experimental data, we obtain the following conclusions.

Based on the fractional order theory and the scale transformation method, the fractal order derivatives are introduced, the Newton body element in the Bingham body is improved, and finally, the anthracite creep model with a fractal damage order is established, and the anthracite creep equation with damage is derived based on the basic element obtained.

The experimental creep data for different damage contents under different loading stresses were obtained through a series of experiments. We find that the initial and accelerated creep of anthracite coal differ with damage contents, and there is a specific functional relationship between them.

Based on the experimental data, an inverse analysis of the relevant parameters of the model was carried out. The results showed that the inverse correlation was >0.9, which proved the reasonability and validity of the model. The sensitivity of the model parameters was also analyzed, and the results showed that the viscosity coefficient η_2 and the damage factor A control the time of the model entering the accelerated creep phase. The order q controls the rate of the accelerated creep phase of the model.

Author Contributions: G.L.: Conceptualization, Data curation, Project management, Roles/Writing—original draft. G.Y.: Funding acquisition, Supervision, Writing—review & editing. S.K.: Funding acquisition, Supervision, Writing—review & editing. X.B.: Writing—review & editing, Data curation. C.D.: Data curation, Formal analysis, Software. J.L.: Investigation. J.Z.: Investigation. All authors have read and agreed to the published version of the manuscript.

Funding: This research was funded by the National Natural Science Foundation of China (Grant No. 51974195) and supported by Shanxi Provincial Department of Education's 2022 Scientific and Technological Innovation Plan for Colleges and Universities in Shanxi Province-Project No.: 2022L055 and project support from Shanxi Science and Technology Department's 2022 Basic Research Plan (Free Exploration)-Project No.: 20220302122099.

Institutional Review Board Statement: Not applicable.

Informed Consent Statement: Not applicable.

Data Availability Statement: The authors do not have permission to share data.

Conflicts of Interest: The authors declare that they have no known competing financial interests or personal relationships that could have appeared to influence the work reported in this paper.

References

1. Gao, Y.; Gao, F.; Zhang, Z.; Zhang, T. Visco-elastic-plastic model of deep underground rock affected by temperature and humidity. *Min. Sci. Technol.* **2010**, *20*, 183–187. [CrossRef]
2. Malan, D.F. Time-dependent Behaviour of Deep Level Tabular Excavations in Hard Rock. *Rock Mech. Rock Eng.* **1999**, *32*, 123–155. [CrossRef]
3. ItÔ, H. 30—The Phenomenon and Examples of Rock Creep. In *Rock Testing and Site Characterization*; Hudson, J.A., Ed.; Pergamon: Oxford, UK, 1993; pp. 693–708. [CrossRef]
4. Zhang, Y.; Xu, W.-Y.; Shao, J.-F.; Zhao, H.-B.; Wang, W. Experimental investigation of creep behavior of clastic rock in Xiangjiaba Hydropower Project. *Water Sci. Eng.* **2015**, *8*, 55–62. [CrossRef]
5. Gao, Y.; Gao, F.; Manchu Ronald, Y. Rock creep modeling based on discontinuous deformation analysis. *Int. J. Min. Sci. Technol.* **2013**, *23*, 757–761. [CrossRef]
6. Boukharov, G.N.; Chanda, M.W.; Boukharov, N.G. The three processes of brittle crystalline rock creep. *Int. J. Rock Mech. Min. Sci. Geomech. Abstr.* **1995**, *32*, 325–335. [CrossRef]
7. Xu, T.; Xu, Q.; Deng, M.; Ma, T.; Yang, T.; Tang, C.-A. A numerical analysis of rock creep-induced slide: A case study from Jiweishan Mountain, China. *Environ. Earth Sci.* **2014**, *72*, 2111–2128. [CrossRef]
8. Zhao, Y.; Zhang, L.; Wang, W.; Wan, W.; Li, S.; Ma, W.; Wang, Y. Creep Behavior of Intact and Cracked Limestone under Multi-Level Loading and Unloading Cycles. *Rock Mech. Rock Eng.* **2017**, *50*, 1409–1424. [CrossRef]
9. Yang, L.; Li, Z.-D. Inverse Analysis of Rock Creep Model Parameters Based on Improved Simulated Annealing Differential Evolution Algorithm. *Geotech. Geol. Eng.* **2019**, *37*, 639–649. [CrossRef]
10. Chang, Z.; Gao, H.; Huang, F.; Chen, J.; Huang, J.; Guo, Z. Study on the creep behaviours and the improved Burgers model of a loess landslide considering matric suction. *Nat. Hazards* **2020**, *103*, 1479–1497. [CrossRef]
11. Xing, Y.; Kulatilake, P.H.S.W.; Sandbak, L.A. Investigation of Rock Mass Stability around the Tunnels in an Underground Mine in USA Using Three-Dimensional Numerical Modeling. *Rock Mech. Rock Eng.* **2018**, *51*, 579–597. [CrossRef]
12. Li, P.; Yan, L.; Yao, D. Study of Tunnel Damage Caused by Underground Mining Deformation: Calculation, Analysis, and Reinforcement. *Adv. Civ. Eng.* **2019**, *2019*, 4865161. [CrossRef]
13. Ma, J.; Dong, L.; Zhao, G.; Li, X. Qualitative Method and Case Study for Ground Vibration of Tunnels Induced by Fault-Slip in Underground Mine. *Rock Mech. Rock Eng.* **2019**, *52*, 1887–1901. [CrossRef]
14. Do, N.A.; Dias, D.; Dinh, V.D.; Tran, T.T.; Dao, V.C.; Dao, V.D.; Nguyen, P.N. Behavior of noncircular tunnels excavated in stratified rock masses—Case of underground coal mines. *J. Rock Mech. Geotech. Eng.* **2019**, *11*, 99–110. [CrossRef]
15. Liu, M.; Liu, F.-Z.; Huang, R.-Q.; Pei, X.-J. Deep-seated large-scale toppling failure in metamorphic rocks: A case study of the Erguxi slope in southwest China. *J. Mt. Sci.* **2016**, *13*, 2094–2110. [CrossRef]
16. Borrelli, L.; Gullà, G. Tectonic constraints on a deep-seated rock slide in weathered crystalline rocks. *Geomorphology* **2017**, *290*, 288–316. [CrossRef]
17. Qian, Q.; Zhou, X. Non-euclidean continuum model of the zonal disintegration of surrounding rocks around a deep circular tunnel in a non-hydrostatic pressure state. *J. Min. Sci.* **2011**, *47*, 37–46. [CrossRef]
18. You, S.; Ji, H.; Zhang, Z.; Zhang, C. Damage Evaluation for Rock Burst Proneness of Deep Hard Rock under Triaxial Cyclic Loading. *Adv. Civ. Eng.* **2018**, *2018*, 8193638. [CrossRef]
19. Yin, G.; Jiang, C.; Wang, J.G.; Xu, J. Combined Effect of Stress, Pore Pressure and Temperature on Methane Permeability in Anthracite Coal: An Experimental Study. *Transp. Porous Media* **2013**, *100*, 1–16. [CrossRef]
20. Falaleev, G.N. Rock creep degree assessment. *J. Min. Sci.* **2010**, *46*, 34–37. [CrossRef]
21. Khoshghalb, A. On Creep Laboratory Tests in Soil Mechanics. In *Multiphysical Testing of Soils and Shales*; Laloui, L., Ferrari, A., Eds.; Springer: Berlin/Heidelberg, Germany, 2013; pp. 255–260.
22. Wu, C.Z.; Chen, Q.S.; Basack, S.; Xu, R.Q.; Shi, Z.M. Biaxial Creep Test Study on the Influence of Structural Anisotropy on Rheological Behavior of Hard Rock. *J. Mater. Civ. Eng.* **2016**, *28*, 04016104. [CrossRef]
23. Mansouri, H.; Ajalloeian, R. Mechanical behavior of salt rock under uniaxial compression and creep tests. *Int. J. Rock Mech. Min. Sci.* **2018**, *110*, 19–27. [CrossRef]
24. Peng, G.; Chen, Z.Q.; Chen, J.R. Research on Rock Creep Characteristics Based on the Fractional Calculus Meshless Method. *Adv. Civ. Eng.* **2018**, *2018*, 1472840. [CrossRef]
25. Huang, W.P.; Xing, W.B.; Chen, S.J.; Liu, Y.; Wu, K. Experimental Study on Sedimentary Rock's Dynamic Characteristics under Creep State Using a New Type of Testing Equipment. *Adv. Mater. Sci. Eng.* **2017**, *2017*, 7623086. [CrossRef]
26. Liu, X.R.; Yang, X.; Wang, J.B. A Nonlinear Creep Model of Rock Salt and Its Numerical Implement in FLAC(3D). *Adv. Mater. Sci. Eng.* **2015**, *2015*, 285158. [CrossRef]

27. Zhu, W.C.; Wei, J.; Niu, L.L.; Li, S.; Li, S.H. Numerical Simulation on Damage and Failure Mechanism of Rock under Combined Multiple Strain Rates. *Shock. Vib.* **2018**, *2018*, 4534250. [CrossRef]
28. Zhang, G.X.; Lei, Z.Q.; Cheng, H. Shear Creep Simulation of Structural Plane of Rock Mass Based on Discontinuous Deformation Analysis. *Math. Probl. Eng.* **2017**, *2017*, 1582825. [CrossRef]
29. Tang, H.; Wang, D.P.; Huang, R.Q.; Pei, X.J.; Chen, W.L. A new rock creep model based on variable-order fractional derivatives and continuum damage mechanics. *Bull. Eng. Geol. Environ.* **2018**, *77*, 375–383. [CrossRef]
30. Liu, L.; Wang, G.M.; Chen, J.H.; Yang, S. Creep experiment and rheological model of deep saturated rock. *Trans. Nonferrous Met. Soc. China* **2013**, *23*, 478–483. [CrossRef]
31. Wan, L.H.; Cao, P.; Huang, Y.H.; Wang, Y.X.; Zhang, X.Y. Creep Test of Hard Rock and the Modified Generalized Kelvin Creep Model. In Proceedings of the International Conference on Civil Engineering and Transportation (ICCET 2011), Jinan, China, 14–16 October 2011; pp. 626–632.
32. Kawada, Y.; Yajima, T.; Nagahama, H. Fractional-order derivative and time-dependent viscoelastic behaviour of rocks and minerals. *Acta Geophys.* **2013**, *61*, 1690–1702. [CrossRef]
33. Li, L.; Qiang, Y.; Li, S.; Yang, Z. Research on Slope Deformation Prediction Based on Fractional-Order Calculus Gray Model. *Adv. Civ. Eng.* **2018**, *2018*, 9526216. [CrossRef]
34. Ezzat, M.A.; El Karamany, A.S.; Fayik, M.A. Fractional order theory in thermoelastic solid with three-phase lag heat transfer. *Arch. Appl. Mech.* **2012**, *82*, 557–572. [CrossRef]
35. Rinaldi, A.; Mastilovic, S. The Krajcinovic approach to model size dependent fracture in quasi-brittle solids. *Mech. Mater.* **2014**, *71*, 21–33. [CrossRef]
36. Yang, S.; Jiang, Y. Triaxial mechanical creep behavior of sandstone. *Min. Sci. Technol.* **2010**, *20*, 339–349. [CrossRef]
37. Zhu, W.; Li, S.; Li, S.; Niu, L. Influence of Dynamic Disturbance on the Creep of Sandstone: An Experimental Study. *Rock Mech. Rock Eng.* **2019**, *52*, 1023–1039. [CrossRef]
38. Yu, M.; Mao, X.; Hu, X. Shear creep characteristics and constitutive model of limestone. *Int. J. Min. Sci. Technol.* **2016**, *26*, 423–428. [CrossRef]
39. Liu, Y.; Liu, C.; Kang, Y.; Wang, D.; Ye, D. Experimental research on creep properties of limestone under fluid–solid coupling. *Environ. Earth Sci.* **2015**, *73*, 7011–7018. [CrossRef]
40. Taherynia, M.H.; Fatemi Aghda, S.M.; Fahimifar, A. In-Situ Stress State and Tectonic Regime in Different Depths of Earth Crust. *Geotech. Geol. Eng.* **2016**, *34*, 679–687. [CrossRef]